Steel and Composite Structures, *Vol. 32, No. 2 (2019) 253-264*
DOI: https://doi.org/10.12989/scs.2019.32.2.253

Combination resonance analysis of FG porous cylindrical shell under two-term excitation

Habib Ahmadi * and Kamran Foroutan [a]

Faculty of Mechanical Engineering, Shahrood University of Technology, Shahrood, Iran

(*Received February 23, 2019, Revised June 8, 2019, Accepted June 10, 2019*)

Abstract. This paper presents the combination resonances of FG porous (FGP) cylindrical shell under two-term excitation. The effect of structural damping on the system response is also considered. With regard to classical plate theory of shells, von-Kármán equation and Hook law, the relations of stress-strain is derived for shell. According to the Galerkin method, the discretized motion equation is obtained. The combination resonances are obtained by using the method of multiple scales. Four types of FGP distributions consist of uniform porosity, non-symmetric porosity soft, non-symmetric porosity stiff and symmetric porosity distribution are considered. The influence of various porosity distributions, porosity coefficients of cylindrical shell and amplitude excitations on the combination resonances for FGP cylindrical shells is investigated.

Keywords: cylindrical shell; FG porous material; combination resonance; multiple scales method; two-term excitation

1. Introduction

The FGP cylindrical shells are used extensively in a wide range of engineering applications, including porous electrodes, heat exchangers, energy absorbing systems, electromagnetic shielding, construction materials and sound absorbers.

Some studies are concentrated the various analyses of functionally graded (FG) and composite structures. The bending problem of a FG cantilever beam subjected to uniformly distributed load was investigated by Daouadji and Adim (2016b). Benferhat *et al*. (2016a) studied the free vibration analysis of FG plates resting on an elastic foundation using higher-order shear deformation theory. Adim *et al*. (2016e) investigated the static behavior and free vibration of laminated composite plates using a refined shear deformation theory. The bending analysis of an imperfect FG plates subjected to the hygro-thermo-mechanical loading was reported by Daouadji *et al*. (2016a). Daouadji and Adim (2016a) addressed an analytical approach for buckling of the FG plates. Adim *et al*. (2016a) presented the buckling behavior of anti-symmetric cross-ply laminated composite plates with different boundary conditions utilizing a refined higher order exponential shear deformation theory. Thermal buckling analysis of FG sandwich plates with clamped boundary conditions was investigated by Abdelhak *et al*. (2016). Adim and Daouadji (2016) studied the effects of thickness stretching in FG plates using a quasi-3D higher order shear deformation theory. Daouadji *et al*. (2016b) addressed a novel higher order shear deformation theory based on the neutral surface concept of FG plate under transverse load. Adim *et al*. (2016b) presented the buckling and free vibration analysis of laminated composite plates using an efficient and simple higher order shear deformation theory. An efficient and simple higher order shear deformation theory for bending analysis of composite plates under various boundary conditions were investigated by Adim *et al*. (2016d). Adim *et al*. (2016c) reported the static, buckling, and free vibration of laminated composite plates using a refined shear deformation theory.

Tesar (1985) analyzed the nonlinear resonance response (three dimensional analyses) for thin shells using the FETM method. Alijani *et al*. (2011), via the multiple scales method, investigated the resonant analysis of the shallow shells with FG material. The cylindrical shells vibrations with FG material under external and parametric excitations were analyzed by Sheng and Wang (2018b). Du and Li (2014) addressed the cylindrical shells resonance with FG material under thermal loading. Li *et al*. (2018) studied the parametric resonant analysis of the FG cylindrical shell under thermal loading. Sheng and Wang (2018a) addressed the primary resonant response and dynamic stability of stiffened cylindrical shells with FG material. The internal resonance of imperfect circular cylindrical shell under transversally excitation was studied by Rodrigues *et al*. (2017). Breslavsky and Amabili (2018) presented the multiple internal resonances subjected to the multi-harmonic excitation. Rossikhin and Shitikova (2015) analyzed the nonlinear vibration of the cylindrical shell consist of fractionally damped with a three-to-one internal resonance. The resonant analysis of composite laminated circular cylindrical shell was studied by Zhang *et al*. (2018). In this work, the steady-state response was obtained by using the shooting method. Abe *et al*. (2007) analyzed the internal resonance response of clamped shallow shells.

∗Corresponding author, Ph.D.,
E-mail: habibahmadif@shahroodut.ac.ir
[a] Ph.D. Student

http://www.techno-press.org/?journal=scs&subpage=6
ISSN: 1229-9367 (Print), 1598-6233 (Online)

Ahmadi and Foroutan (2019) investigated the primary resonant behavior of functionally graded cylindrical shells with spiral stiffeners by utilizing the multiple scales method. Also, Ahmadi (2018) studied the primary resonant behavior of imperfect FG cylindrical shells with spiral stiffeners rested on the nonlinear elastic foundation.

Some studies are paid attention to various analyses of porous structures, the mechanical and thermal stability analysis was analyzed by Mojahedin *et al*. (2014) for a circular porous plate. The effect of porosity on the bending and free vibration response of FG plates resting on the elastic foundations was studied by Benferhat *et al*. (2016b). Also, Benferhat *et al*. (2016c) investigated the static analysis of the FG plate with porosities. Magnucki et al. (2006) presented the bending and buckling of a rectangular porous plate. Galeban *et al*. (2016) investigated the free vibration of thin beams with FG porous material. Chen *et al*. (2015) analyzed the elastic buckling and static bending of shear deformable FGP beam. Kitipornchai *et al*. (2017) presented the free vibration and elastic buckling of FGP beams reinforced by graphene platelets. Zhao *et al*. (2019a) presented the free vibration analyses of moderately thick FGP deep curved and straight beams. Deflection and vibration analysis of higher-order shear deformable compositionally graded porous plate using the finite element method addressed by Ebrahimi and Habibi (2016). Zhao *et al*. (2019d) analyzed the dynamics behavior of FGP circular, annular and sector plates with general elastic restraints. Mirjavadi *et al*. (2017) presented the thermo-mechanical vibration analysis of two dimensional nanobeam with FG porous material. Yang *et al*. (2018) reported the buckling and free vibration analyses of functionally graded graphene reinforced porous nanocomposite plates based on Chebyshev-Ritz method. Zhao *et al*. (2019b) studied the free vibrations behavior of FGP rectangular plate with uniform elastic boundary conditions. The free harmonic wave propagation for composite cylindrical shell with porous materials was investigated by Daneshjou *et al*. (2011). Thermal buckling analysis of nanobeam with FG porous material was addressed by Karami *et al*. (2018). Belica *et al*. (2011) investigated the dynamic stability of a cylindrical shell with metal foam material under axial compression and external pressure. Also, Belica and Magnucki (2006) studied the stability of a porous cylindrical shell dynamic.

In reported works mentioned above, the researchers have not addressed the resonant behavior of porous cylindrical shell with FG material. Some researches have been performed the resonant analysis of cylindrical shells with FG porous material. In this field, Wang and Wu (2017) studied the free vibration of FGP cylindrical shell by means of a sinusoidal shear deformation theory. Guan *et al*. (2019) investigated a general vibration analysis of FGP structure elements of revolution with general elastic restraints. The free vibration analysis of size-dependent FGP cylindrical microshells in thermal environment was investigated by Ghadiri and SafarPour (2017). Zare Jouneghani *et al*. (2017) presented the free vibration analysis of FGP doubly-curved shells based on the first order shear deformation theory. Zhao *et al*. (2019e) analyzed the vibration behavior of the FGP doubly-curved panels and shells of revolution by using a semi-analytical method. The vibration behavior of the FG graphene reinforced porous nanocomposite cylindrical shell was addressed by Dong *et al*. (2018). Li *et al*. (2018) presented the free vibration analysis of FG porous cylindrical shell with arbitrary boundary restraints. Gao *et al*. (2018) analyzed the primary resonance of cylindrical shells with FG porous material.

Review of the literature shows that there is no study on the combination resonances of FG porous cylindrical shells under two-term excitation. This subject is the main reason to motivate author for defining present study. Therefore, the novelties in this work are as: (1) combination resonances formulation are analytically derived via the method of multiple scales for FGP cylindrical shell, (2) the effect of four type of porosity distributions consist of uniform porosity, non-symmetric porosity soft, non-symmetric porosity stiff and symmetric porosity distribution are analyzed, (3) the effect of porosity coefficients of cylindrical shell and amplitude excitations on combination resonance of system is investigated, (4) the effect of various geometrical characteristics such as radios-to-thickness and length-to-radios ratios is studied. The organization of the present paper is as follows. Section 2 presents the basic formulation. In section 2.1, the schematic of FG porous cylindrical shell is shown and the properties of shell are expressed. In section 2.2, the theoretical formulation is derived, and in section 2.2.1, the governing equation is obtained based on theory of classical shell and von Kármán equation. In section 2.2.2, using the Galekin method, the motion equations are discretized, and in section 2.2.3, the combination resonances for two-term excitation via the multiple scales method is derived. Section 3 shows the numerical results, and in section 3.1, the validation of the present approach is illustrated. In section 3.2, the results of combination resonances are shown, and finally the conclusions of this study are expressed.

2. The basic formulation

2.1 FG porous cylindrical shell

A schematic view of a FG porous (FGP) cylindrical shell with its coordinate system (x, y, z) is shown in Fig. 1, where x, z and $y = R\theta$ are the axial, radial and circumferential direction, respectively. The point "*O*" in Fig. 1, shows the coordinate system origin. The cylindrical shell has thickness h, axial length L and radius R.

In this paper, four FGP distributions types are considered which are illustrated in Fig. 2. The mass density and Young's modulus of metal foam materials can be expressed in the following form (Belica and Magnucki 2006, Belica *et al*. 2011, Mojahedin *et al*. 2014, Wang and Wu 2017, Gao *et al*. 2018, Zhao *et al*. 2019c)

Type1: Uniform porosity distribution

$$\begin{aligned} E(z) &= E_{\max} - \zeta N_0 E_{\max} \\ \rho(z) &= \rho_{\max} - \zeta N_m \rho_{\max} \end{aligned} \tag{1}$$

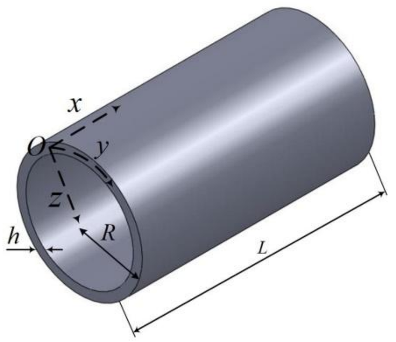

Fig. 1 Configuration of FGP cylindrical shell

Type2: Non-symmetric porosity soft distribution

$$
\begin{aligned}
E(z) &= E_{\max} - \sin\left(\frac{\pi z}{2h} + \frac{\pi}{4}\right) N_0 E_{\max} \\
\rho(z) &= \rho_{\max} - \sin\left(\frac{\pi z}{2h} + \frac{\pi}{4}\right) N_m \rho_{\max}
\end{aligned} \tag{2}
$$

Type2: Non-symmetric porosity stiff distribution

$$
\begin{aligned}
E(z) &= E_{\max} - \cos\left(\frac{\pi z}{2h} + \frac{\pi}{4}\right) N_0 E_{\max} \\
\rho(z) &= \rho_{\max} - \cos\left(\frac{\pi z}{2h} + \frac{\pi}{4}\right) N_m \rho_{\max}
\end{aligned} \tag{3}
$$

Type1: Symmetric porosity distribution

$$
\begin{aligned}
E(z) &= E_{\max} - \cos\left(\frac{\pi z}{h}\right) N_0 E_{\max} \\
\rho(z) &= \rho_{\max} - \cos\left(\frac{\pi z}{h}\right) N_m \rho_{\max}
\end{aligned} \tag{4}
$$

where $-h/2 \le z \le h/2$ and. $\rho_{\max}$ and $E_{\max}$ are the maximum of mass density and Young's modulus, respectively. N_0 and N_m are the porosity coefficients of cylindrical shell and mass density which can be calculated as

$$
\begin{aligned}
N_0 &= 1 - \frac{E_{\min}}{E_{\max}}; \quad 0 < N_0 < 1 \\
N_m &= 1 - \sqrt{1 - N_0}
\end{aligned} \tag{5}
$$

Also, ζ in Eq. (1) for type 1 is given by

$$
\zeta = \frac{1}{N_0} - \frac{1}{N_0}\left(1 - \frac{2N_m}{\pi}\right)^2 \tag{6}
$$

2.2 The theoretical formulation

2.2.1 Governing equations

According to the strain-displacement (von Kármán) relations (Brush and Almroth 1975), the strain components on the middle surface of shells are given by (Djoudi and Bahai 2003)

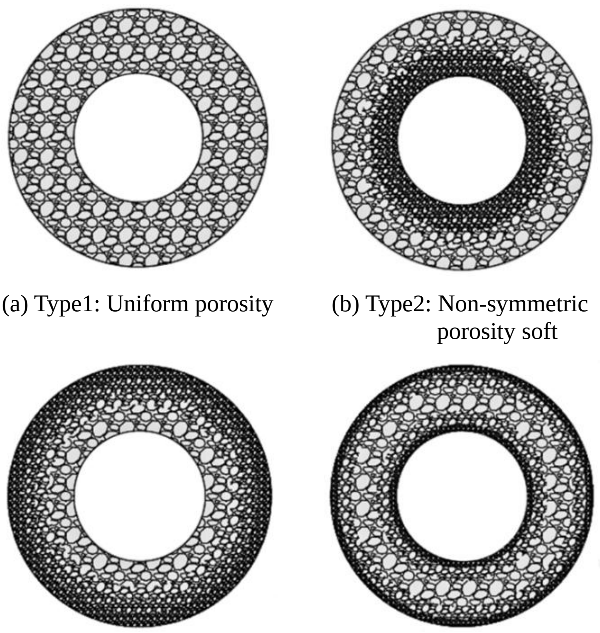

(a) Type1: Uniform porosity

(b) Type2: Non-symmetric porosity soft

(c) Type3: Non-symmetric porosity stiff

(d) Type4: Symmetric porosity

Fig. 2 Cross-section of FGP cylindrical shell for various porosity distributions

$$
\begin{aligned}
\varepsilon_x^0 &= u_{,x} + \frac{1}{2} w_{,x}^2 \\
\varepsilon_y^0 &= v_{,y} - \frac{w}{R} + \frac{1}{2} w_{,y}^2 \\
\gamma_{xy}^0 &= u_{,y} + v_{,x} + w_{,x} w_{,y} \\
\kappa_x &= w_{,xx}, \ \kappa_y = w_{,yy}, \ \kappa_{xy} = w_{,xy}
\end{aligned} \tag{7}
$$

where $w = w(x,y)$, $u = u(x,y)$ and $v = v(x,y)$ are the displacement components along z, x and y axes, respectively. γ_{xy}^0 is shear strain, and ε_y^0, ε_x^0 are normal strains. Also, the terms $\chi_x, \chi_y, \chi_{xy}$ are the shell curvatures change and twist.

The strain components are obtained across the shell thickness at the middle surface as follows (Zhang *et al*. 2017, Pradhan *et al*. 2000)

$$
\varepsilon_x = \varepsilon_x^0 - z\,\kappa_x, \ \varepsilon_y = \varepsilon_y^0 - z\,\kappa_y, \ \gamma_{xy} = \gamma_{xy}^0 - 2z\,\kappa_{xy} \tag{8}
$$

The compatibility equation according to Eq. (2) can be written as follows

$$
\varepsilon_{x,yy}^0 + \varepsilon_{y,xx}^0 - \gamma_{xy,xy}^0 = -\frac{1}{R} w_{,xx} + \left(w_{,xy}\right)^2 - w_{,xx} w_{,yy} \tag{9}
$$

The stress-strain relations based on the Hooke low for FGP cylindrical shell are defined as (Loy *et al*. 1999)

$$
\begin{aligned}
\left(\sigma_x, \sigma_y\right) &= \frac{E(z)}{1-\nu^2}\left[\left(\varepsilon_x, \varepsilon_y\right) + \nu\left(\varepsilon_y, \varepsilon_x\right)\right] \\
\tau_{xy} &= \frac{E(z)}{2(1+\nu)} \gamma_{xy}
\end{aligned} \tag{10}
$$

where ν is the Poisson's ratio. σ_y, σ_x are the normal stress and τ_{xy} is the shear stress of cylindrical shell.

To derive the resultant moments (M_x, M_y, M_{xy}) and forces (N_x, N_y, N_{xy}) for FGP cylindrical shell, the stress-strain equations (Eq. (10)) are integrated through the thickness as

Resultant force

$$\begin{aligned} N_x &= J_{11}\varepsilon_x^0 + J_{12}\varepsilon_y^0 - J_{14}\chi_x - J_{15}\chi_y \\ N_y &= J_{21}\varepsilon_x^0 + J_{22}\varepsilon_y^0 - J_{24}\chi_x - J_{25}\chi_y \\ N_{xy} &= J_{33}\gamma_{xy}^0 - 2J_{36}\chi_{xy} \end{aligned} \tag{11}$$

Resultant moment

$$\begin{aligned} M_x &= J_{14}\varepsilon_x^0 + J_{15}\varepsilon_y^0 - J_{41}\chi_x - J_{42}\chi_y \\ M_y &= J_{24}\varepsilon_x^0 + J_{25}\varepsilon_y^0 - J_{51}\chi_x - J_{52}\chi_y \\ M_{xy} &= J_{36}\gamma_{xy}^0 - 2J_{63}\chi_{xy} \end{aligned} \tag{12}$$

where J_{ij} are the coupling, bending and extensional stiffness components of FGP system that are presented in Appendix. With regard to Eq. (11), the strain components can be rewritten as

$$\begin{aligned} \varepsilon_x^0 &= J_{22}^* N_x - J_{12}^* N_y + J_{11}^{**}\chi_x + J_{12}^{**}\chi_y \\ \varepsilon_y^0 &= J_{11}^* N_y - J_{21}^* N_x + J_{21}^{**}\chi_x + J_{22}^{**}\chi_y \\ \gamma_{xy}^0 &= J_{33}^* N_{xy} + 2J_{36}^{**}\chi_{xy} \end{aligned} \tag{13}$$

Then, Eq. (13) is substituted into Eq. (12) in the following form

$$\begin{aligned} M_x &= A_{11}^* N_x + A_{21}^* N_y - A_{11}^{**}\chi_x - A_{12}^{**}\chi_y \\ M_y &= A_{12}^* N_x + A_{22}^* N_y - A_{21}^{**}\chi_x - A_{22}^{**}\chi_y \\ M_{xy} &= A_{36}^* N_{xy} - 2A_{36}^{**}\chi_{xy} \end{aligned} \tag{14}$$

The equilibrium equations of cylindrical shells with regard to theory of classical shell are as (Volmir 1972, Bich *et al*. 2013, Ghiasian *et al*. 2013)

$$\begin{aligned} & N_{x,x} + N_{xy,y} = 0 \\ & N_{xy,x} + N_{y,y} = 0 \\ & M_{x,xx} + 2M_{xy,xy} + M_{y,yy} + N_x w_{,xx} + 2N_{xy} w_{,xy} \\ & \quad + N_y\left(w_{,yy} + \frac{1}{R}\right) + q(t) = \rho_1 w_{,tt} + 2\rho_1 \hat{c} w_{,t} \end{aligned} \tag{15}$$

where $q(t) = Q_1 \cos(\Omega_1 t + \theta_1) + Q_2 \cos(\Omega_2 t + \theta_2)$ is the harmonic excitation, $\hat{c}$ is coefficient of damping and mass density ρ_1 are

$$\rho_1 = \int_{-h/2}^{h/2} \rho(z)\, dz \tag{16}$$

With regard to the first two Eq. (15), stress function (φ) is defined as

$$N_x = \varphi_{yy},\ N_y = \varphi_{xx},\ N_{xy} = -\varphi_{xy} \tag{17}$$

By substituting Eq. (13) in Eq. (9) and Eq. (14) in third part of Eq. (15) and then by utilizing Eq. (7) and (17), the following equations of system can be derived as

$$\begin{aligned} & J_{11}^*\varphi_{,xxxx} + \left(J_{33}^* - J_{12}^* + J_{21}^*\right)\varphi_{,xxyy} + J_{22}^*\varphi_{,yyyy} + J_{21}^{**} w_{,xxxx} \\ & + \left(J_{11}^{**} + J_{22}^{**} - 2J_{36}^{**}\right) w_{,xxyy} + J_{12}^{**} w_{,yyyy} + \frac{1}{R} w_{,xx} \\ & + \left[w_{,xy}^2 - w_{,xx} w_{,yy}\right] - 2w_{,xy} + w_{,xx} + w_{,yy} = 0 \end{aligned} \tag{18}$$

$$\begin{aligned} & \rho_1 w_{,tt} + 2\rho_1 \hat{c} w_{,t} + A_{11}^{**} w_{,xxxx} + \left(A_{12}^{**} + A_{21}^{**} + 4A_{36}^{**}\right) w_{,xxyy} \\ & + A_{22}^{**} w_{,yyyy} - A_{21}^*\varphi_{,xxxx} - \left(A_{11}^* + A_{22}^* - 2A_{36}^*\right)\varphi_{,xxyy} \\ & - A_{12}^*\varphi_{,yyyy} - \frac{\varphi_{,xx}}{R} - \varphi_{,yy} w_{,xx} + 2\varphi_{,xy} w_{,xy} - \varphi_{,xx} w_{,yy} \\ & - Q_1 \cos(\Omega_1 t + \theta_1) - Q_2 \cos(\Omega_2 t + \theta_2) = 0 \end{aligned} \tag{19}$$

2.2.2 Discretization of the equation of motion

The FGP cylindrical shell is supposed to be the simply supported. According to boundary condition, the deflection of shells is considered in the following form for single mode (Volmir 1972, Bich *et al*. 2012, Shen and Xiang 2012, Ahmadi and Foroutan 2019)

$$w(x, y, t) = W_{mn}(t) \sin\frac{m\pi x}{L} \sin\frac{ny}{R} \tag{20}$$

where n and m are the number of full and half wave in the circumferential and axial directions, respectively. Also, $W_{mn}(t)$ represent the deflection amplitude.

To obtain the stress function φ, the Eq. (20) is substituted into Eq. (18) and then resultant equation is solved. In the following, the obtained stress function φ and w (from Eq. (20)) are substituted in Eq. (19), then, the Galerkin method is applied and the discretized equation of motion is obtained as

$$\begin{aligned} & \ddot{W}_{mn} + 2\hat{c}\dot{W}_{mn} + \omega_{mn}^2 W_{mn} + \hat{a}_2 W_{mn}^3 \\ & = k_1 \cos(\Omega_1 t + \theta_1) + k_2 \cos(\Omega_2 t + \theta_2) \end{aligned} \tag{21}$$

where $\hat{a}_2$ is the constant coefficient that this parameter is defined in the next sub-section and ω_{mn} is the natural frequency of cylindrical shell as follows

$$\omega_{mn} = \sqrt{\frac{1}{L^4\rho_1}\left(D + \frac{BB^*}{A}\right)},\ \ k_1 = \frac{Q_1}{L^4\rho_1},\ \ k_2 = \frac{Q_2}{L^4\rho_1} \tag{22}$$

where B, A, D and B^* are presented in Appendix.

2.2.3 Combination resonances for two-term excitation

For analyzing the combination resonances, the multiple scales method is used. Therefore, by considering Eq. (21), the parameters $\hat{c}$ and $\hat{a}_2$ are presented as

$$\hat{c} = \epsilon c;\ \ \hat{a}_2 = \epsilon a_2 \tag{23}$$

where $\epsilon \ll 1$ is the perturbation parameter and a_2 is as follows

$$a_2 = G / L^4 \rho_1 \tag{24}$$

where G is defined in Appendix.

Substituting the Eq. (23) into (21), the equation of motion can be written as

$$\ddot{W}_{mn} + 2\epsilon c\dot{W}_{mn} + \omega_{mn}^2 W_{mn} + \epsilon a_2 W_{mn}^3 = k_1 \cos(\Omega_1 t + \theta_1) + k_2 \cos(\Omega_2 t + \theta_2) \tag{25}$$

With regard to the multiple scales method, the solution for Eq. (25) is considered as

$$\mathrm{W}(t, \epsilon) = W_0(T_0, T_1) + \epsilon W_1(T_0, T_1) + \cdots \tag{26}$$

where the new time independent variable T_0 and T_1 are defined as

$$T_n = \epsilon^n t; \qquad n = 0,1 \tag{27}$$

In continue, Eq. (26) is substituted in Eq. (25) and then, the coefficients of ϵ^0 and ϵ are set to zero as follows

$$D_0^2 W_0 + \omega_{mn}^2 W_0 = k_1 \cos(\Omega_1 t + \theta_1) + k_2 \cos(\Omega_2 t + \theta_2) \tag{28}$$

$$D_0^2 W_1 + \omega_{mn}^2 W_1 = -2D_0 D_1 W_0 - 2cD_0 W_0 - a_2 W_0^3 \tag{29}$$

where

$$D_n = \frac{\partial}{\partial T_n}; \qquad n = 0,1 \tag{30}$$

The solution of Eq. (28) is obtained as

$$W_0 = A(T_1) e^{i\omega_{mn} T_0} + \Lambda_1 e^{i\Omega_1 T_0} + \Lambda_2 e^{i\Omega_2 T_0} + c.c. \tag{31}$$

In Eq. (31), c.c. is abbreviation for complex conjugate and

$$\Lambda_1 = \frac{k_1 e^{i\theta_1}}{2(\omega_{mn}^2 - \Omega_1^2)}, \quad \Lambda_2 = \frac{k_2 e^{i\theta_2}}{2(\omega_{mn}^2 - \Omega_2^2)} \tag{32}$$

Then, Eq. (31) is substituted in Eq. (29) as follows

$$\begin{aligned}
D_0^2 W_1 + \omega_{mn}^2 W_1 = &-\Big[2i\omega_{mn}\left(A' + \mu A\right) \\
&+3a_2\left(A\Lambda + 2\Lambda_1\bar{\Lambda}_1 + 2\Lambda_2\bar{\Lambda}_2\right)A\Big]e^{i\omega_{mn}T_0} \\
&-\Lambda_1\left[2i\Omega_1 c + 3a_2\left(2A\bar{A} + \Lambda_1\bar{\Lambda}_1 + 2\Lambda_2\bar{\Lambda}_2\right)\right]e^{i\Omega_1 T_0} \\
&-\Lambda_2\left[2i\Omega_1 c + 3a_2\left(2A\bar{A} + 2\Lambda_1\bar{\Lambda}_1 + \Lambda_2\bar{\Lambda}_2\right)\right]e^{i\Omega_2 T_0} \\
&-a_2\Big\{A^3 e^{3i\omega_{mn}T_0} + \Lambda_1^3 e^{3i\Omega_1 T_0} + \Lambda_2^3 e^{3i\Omega_2 T_0} \\
&+3A^2\Lambda_1 e^{i(2\omega_{mn}+\Omega_1)T_0} + 3A^2\Lambda_2 e^{i(2\omega_{mn}+\Omega_2)T_0} \\
&+3A^2\bar{\Lambda}_1 e^{i(2\omega_{mn}-\Omega_1)T_0} + 3A^2\bar{\Lambda}_2 e^{i(2\omega_{mn}-\Omega_2)T_0} \\
&+3A\Lambda_1^2 e^{i(\omega_{mn}+2\Omega_1)T_0} + 3A\Lambda_2^2 e^{i(\omega_{mn}+2\Omega_2)T_0} \\
&+3A\bar{\Lambda}_1^2 e^{i(\omega_{mn}-2\Omega_1)T_0} + 6A\bar{\Lambda}_1\Lambda_2 e^{i(\omega_{mn}-\Omega_1+\Omega_2)T_0} \\
&+6A\Lambda_1\bar{\Lambda}_2 e^{i(\omega_{mn}+\Omega_1-\Omega_2)T_0} + 3\Lambda_1^2\Lambda_2 e^{i(2\Omega_1+\Omega_2)T_0} \\
&+3\Lambda_1^2\bar{\Lambda}_2 e^{i(2\Omega_1-\Omega_2)T_0} + 3\Lambda_1\Lambda_2^2 e^{i(\Omega_1+2\Omega_2)T_0} \\
&+3\bar{\Lambda}_1\Lambda_2^2 e^{i(2\Omega_2-\Omega_1)T_0}\Big\} + \text{c.c.}
\end{aligned} \tag{33}$$

Eq. (33) shows the several resonant combinations that some of them are monofrequency and others are multifrequency characteristic of excitations, respectively. These combinations are in the following form

subharmonic resonance:

$$\omega_{mn} \approx \frac{1}{3}\Omega_k \tag{34}$$

superharmonic resonance:

$$\omega_{mn} \approx 3\Omega_k \tag{35}$$

combination resonance:

$$\begin{aligned}
\omega_{mn} &\approx \left|\pm 2\Omega_l \pm \Omega_k\right| \\
\omega_{mn} &\approx \frac{1}{2}\left(\Omega_l \pm \Omega_k\right)
\end{aligned} \tag{36}$$

where $k, l = 1, 2$. It should be noted that for a multifrequency excitation, several resonant conditions may be occurred simultaneously; i.e., both superharmonic and combination resonances or both subharmonic and superharmonic resonances, etc can occur simultaneously. For a two-term excitation, maximum two resonances can be occurred simultaneously. If excitation frequencies are depicted by Ω_1 and Ω_2 where $\Omega_2 > \Omega_1$, the possible secondary resonances can be occurred in the following form

$$\begin{aligned}
\omega_{mn} &\approx 3\Omega_1 \text{ or } 3\Omega_2 \\
\omega_{mn} &\approx \frac{1}{3}\Omega_1 \text{ or } \frac{1}{3}\Omega_2 \\
\omega_{mn} &\approx \Omega_2 \pm 2\Omega_1 \text{ or } 2\Omega_1 - \Omega_2 \\
\omega_{mn} &\approx 2\Omega_2 \pm \Omega_1 \\
\omega_{mn} &\approx \frac{1}{2}\left(\Omega_2 \pm \Omega_1\right)
\end{aligned} \tag{37}$$

Investigation of these resonances shows that more than one of them occurs simultaneously if

$$\begin{aligned}
&(\text{a})\ \Omega_2 \approx 9\Omega_1 \approx 3\omega_{mn} \\
&(\text{b})\ \Omega_2 \approx \Omega_1 \approx 3\omega_{mn} \\
&(\text{c})\ \Omega_2 \approx \Omega_1 \approx \frac{1}{3}\omega_{mn} \\
&(\text{d})\ \Omega_2 \approx 5\Omega_1 \approx \frac{5}{3}\omega_{mn} \\
&(\text{e})\ \Omega_2 \approx 7\Omega_1 \approx \frac{7}{3}\omega_{mn} \\
&(\text{f})\ \Omega_2 \approx 2\Omega_1 \approx \frac{2}{3}\omega_{mn}
\end{aligned} \tag{38}$$

$$\begin{aligned} &(\mathrm{g})\ \Omega_2 \approx \frac{7}{3}\Omega_1 \approx 7\omega_{mn} \\ &(\mathrm{h})\ \Omega_2 \approx \frac{5}{3}\Omega_1 \approx 5\omega_{mn} \end{aligned} \tag{38}$$

Here, the case $\omega_{mn} \approx \Omega_2 + 2\Omega_1$ is selected. In order to frequency analysis, a detuning parameter σ is introduced that this parameter expresses the nearness $\Omega_2 + 2\Omega_1$ to ω_{mn}. Therefore, the excitation frequency can be written as

$$\omega_{mn} = \Omega_2 + 2\Omega_1 - \epsilon\sigma \tag{39}$$

Eq. (39) is substituted in Eq. (33), and then secular terms must be zero as follows

$$\begin{aligned} &2i\omega_{mn}\left(A' + cA\right) + 3a_2\left(A\Lambda + 2\Lambda_1\bar{\Lambda}_1 + 2\Lambda_2\bar{\Lambda}_2\right)A \\ &\quad + 3a_2\Lambda_1^2\Lambda_2 e^{i\sigma T_1} = 0 \end{aligned} \tag{40}$$

To solve the Eq. (40), A is considered in polar form as

$$A = \frac{1}{2}ae^{i\beta} \tag{41}$$

where β and a are real.

Eq. (41) is substituted in Eq. (40), and then real part and imaginary part are separated as

$$a' = -\mu a - a_2\,\Gamma_1 \sin(\gamma) \tag{42}$$

$$a\gamma' = (\sigma - a_2\,\Gamma_2)a - \frac{3a_2}{8\omega_{mn}}a^3 - a_2\,\Gamma_1\cos(\gamma) \tag{43}$$

where

$$\begin{aligned} &\Gamma_1 = \frac{3}{8}k_1^2 k_2 \omega_{mn}^{-1}\left(\omega_{mn}^2 - \Omega_1^2\right)^{-2}\left(\omega_{mn}^2 - \Omega_2^2\right)^{-1} \\ &\Gamma_2 = \frac{3}{4}\omega_{mn}^{-1}\left[k_1^2\left(\omega_{mn}^2 - \Omega_1^2\right)^{-2} + k_2^2\left(\omega_{mn}^2 - \Omega_2^2\right)^{-2}\right] \\ &\gamma = \sigma T_1 - \beta + 2\theta_1 + \theta_2 \end{aligned} \tag{44}$$

When a' and γ' are equal to zero, the steady-state motion occurs. In this situation, from Eqs. (42) and (43), singular points are obtained. In continue, frequency-response relation is calculated by summing the squares of resultant equations in steady state situation as

$$\left[c^2 + \left(\sigma - a_2\,\Gamma_2 - \frac{3a_2}{8\omega_{mn}}a^2\right)^2\right]a^2 = a_2^2\,\Gamma_1^2 \tag{45}$$

3. Numerical results

3.1 Validation of the present approach

In this sub-section, first, the presented work is compared with the other related works. Then, the numerical method is utilized to compare with the presented analytical method. These validation procedures are addressed as follows.

Table 1 Comparison of the natural frequencies of simply supported ($L = 0.2$ m, $R = 0.1$ m, $h = 0.247 \times 10^{-3}$ m, $m = 1$, $\nu = 0.31$, $E = 7.12 \times 10^{10}$ N/m^2, $\rho = 2796$ kg/m^3)

m	n	Present	Qin *et al*. (2017)		Pellicano (2007)	
				Errors (%)		Errors (%)
1	7	486.0	484.6	0.2	484.6	0.2
1	8	490.3	489.6	0.1	489.6	0.1
1	9	545.8	546.2	0.07	546.2	0.07
1	6	555.8	553.3	0.4	553.3	0.4
1	10	634.8	636.8	0.3	636.8	0.3
1	5	728.5	722.1	0.8	722.1	0.8
1	11	746.6	750.7	0.5	750.7	0.5
1	12	875.5	882.2	0.7	882.2	0.7
2	10	962.3	968.1	0.5	968.1	0.5
2	11	976.6	983.4	0.6	983.4	0.6

Table 2 Comparison of the non-dimensional natural frequencies of simply supported FGP cylindrical shell ($m = 1$)

n	N_0	Present	Wang and Wu (2017)	
				Errors (%)
Symmetric porosity distribution				
1	0.4	1.1935	1.1893	0.3
2	0.4	1.1906	1.1862	0.3
3	0.4	1.1867	1.1818	0.4
1	0.8	1.1693	1.1633	0.5
2	0.8	1.1681	1.1617	0.5
3	0.8	1.1668	1.1599	0.6
Non-symmetric porosity distribution				
1	0.4	1.1637	1.1598	0.3
2	0.4	1.1600	1.1559	0.3
3	0.4	1.1546	1.1501	0.4
1	0.8	1.0548	1.0507	0.4
2	0.8	1.0505	1.0463	0.4
3	0.8	1.0440	1.0396	0.4

(I) Validation based on the comparison with the other works: Table 1 compares the natural frequencies for cylindrical shells that are obtained in this study with similar results which investigated by Qin *et al*. (2017) and Pellicano (2007). Also, Table 2 compares the natural frequencies for FGP cylindrical shells that are obtained in this study with similar results which investigated by Wang and Wu (2017). It is observed that these are a good agreement for the results of present study.

Fig. 3 shows the cylindrical shell natural frequencies that obtained in this study, to compare with the experimentally results reported in Sewall and Naumann (1968). Also, this comparison confirms a good agreement of the results obtained in this paper.

(II) Validation based on the comparison with the numerical method: the numerical method is utilized to compare with analytical method in order to combination resonance analysis of type 4 (Symmetric porosity distribution) for FGP cylindrical shell. In numerical validation, Eq. (21) is solved by means of the Runge-Kutta algorithm (fourth-order). In this method, for various excitations, the maximum amplitude is extracted from the responses (I. C.: $W(0) = 0$ and $\dot{W}(0) = 0$). The curves

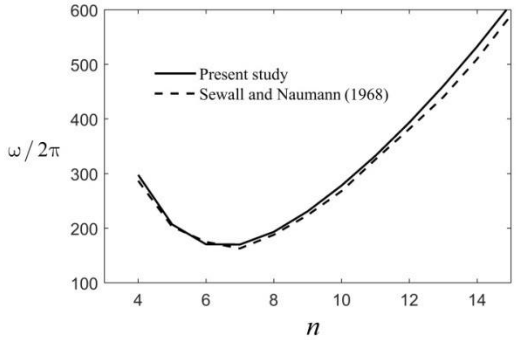

Fig. 3 Comparison of the natural frequencies of cylindrical shell ($m = 1$)

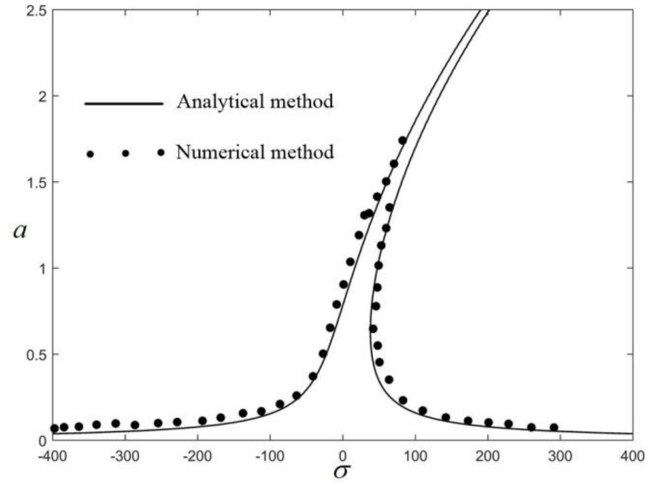

Fig. 4 Analytical and numerical frequency-response curve for type 1 of FGP cylindrical shell

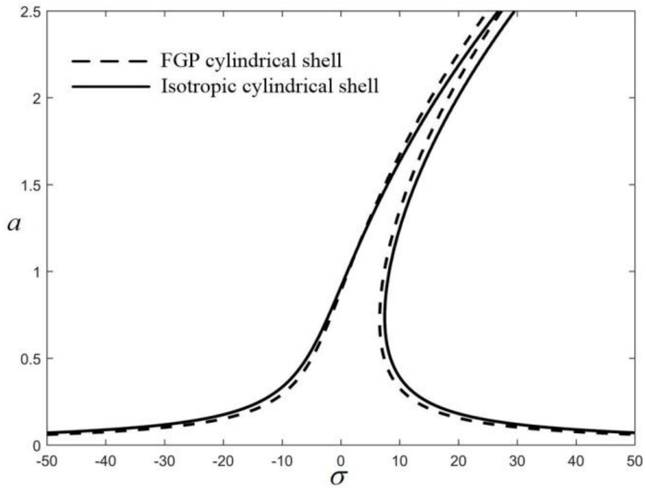

(a) Type1: Uniform porosity distribution

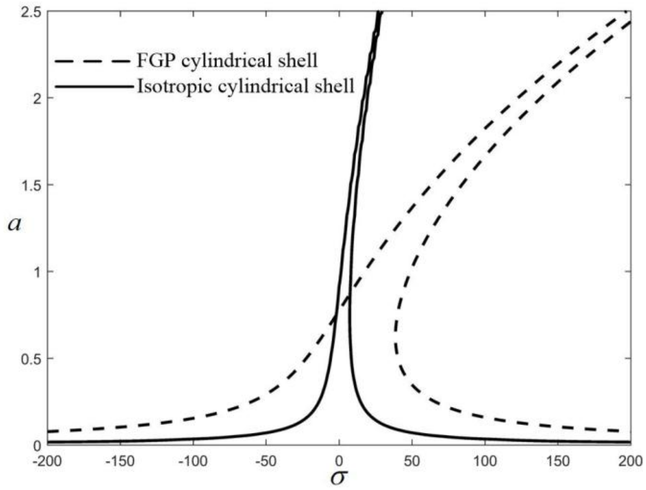

(b) Type2: Non-symmetric porosity soft distribution

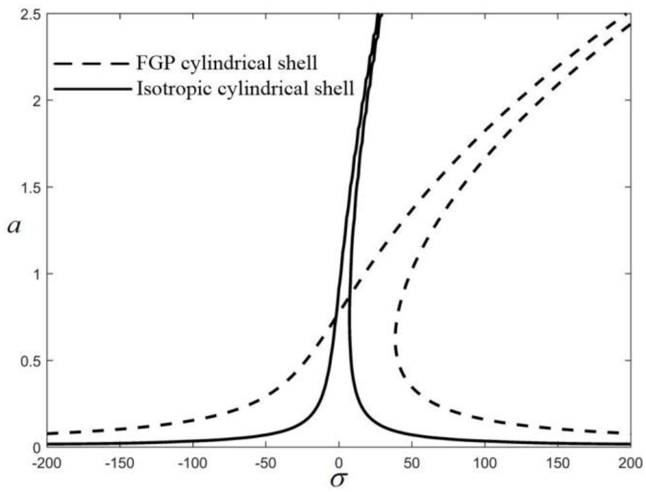

(c) Type3: Non-symmetric porosity stiff distribution

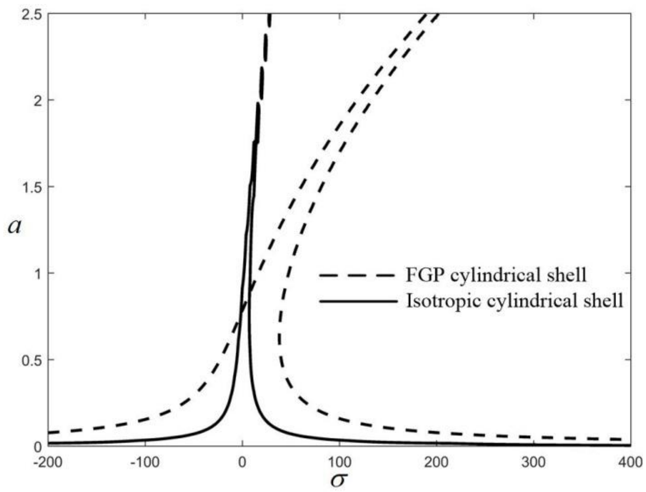

(d) Type4: Symmetric porosity distribution

Fig. 5 Frequency-response curves of FGP cylindrical shells ($N_0 = 0.4$)

Table 3 The material and geometrical parameters of shell

Material parameters	Value	Geometrical characteristics	Value
$E_{\max}$	200 GPa	h	0.25 m
$\rho_{\max}$	$7850\ \mathrm{kg/m^3}$	R	25 m
ν	0.3	L	250 m

of numerical and analytical frequency-response are illustrated in Fig. 4. It can be seen, analytical results are almost similar to the numerical ones. Therefore, this result shows that the numerical simulation verify the analytical method in this paper.

3.2 Combination resonances ($\omega_{mn} \approx \Omega_2 + 2\Omega_1$)

Here, combination resonance responses of FGP cylindrical shell are presented. In this work, $m = 1$ and the Poisson's ratio is considered costatnt. The rest of geometrical characteristics and material parameters of shell are presented in Table 3.

The effect of isotropic and various porosity distributions for shell on the response of amplitude-frequency for combination resonances of system are illustrated in Fig. 5. With regard to these figures, the hardening nonlinearity behavior of FGP cylindrical shell is more than isotropic cylindrical shell except for type1 (uniform porosity distribution).

Fig. 6 shows the influence of porosity coefficients of cylindrical shell on the frequency-response for combination resonances of FGP system. According to this figure, increasing the porosity coefficients of cylindrical shell leads to increasing nonlinearity behavior.

The influence of the excitation amplitudes Γ_1 and Γ_2 on the frequency-response for combination resonances of FGP cylindrical shell is illustrated in Figs. 7 and 8, respectively. As shown in Fig. 7, as a result of increasing Γ_1, the curve of frequency-response is scaled up. Whereas Fig. 8 shows that by increasing Γ_2, the jumping phenomenon is transferred to higher values of σ.

Fig. 9 shows the effect of radius-to-thickness ratio on the frequency-response for combination resonances of FGP system. Considering this figure, by increasing the radius-to-

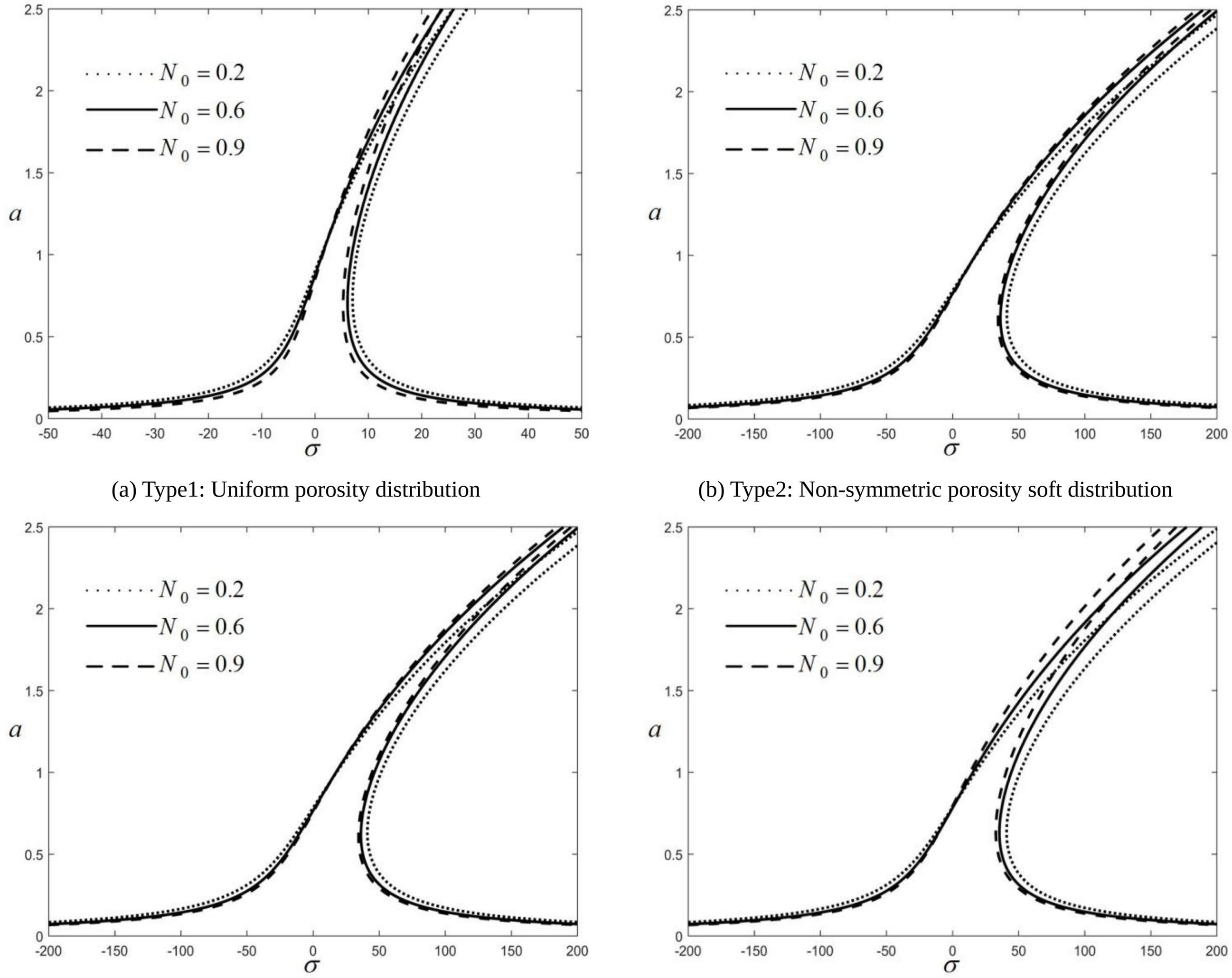

(a) Type1: Uniform porosity distribution

(b) Type2: Non-symmetric porosity soft distribution

(c) Type3: Non-symmetric porosity stiff distribution

(d) Type4: Symmetric porosity distribution

Fig. 6 Frequency-response curves of FGP cylindrical shells thickness ratio, the nonlinearity behavior decreases.

The effect of length-to-radius ratio on the frequency-response for combination resonances of FGP system is $R = 13$, maximum softening nonlinearity is occurred. Also, it can be seen that for $L/R > 13$ or $L/R < 13$, the hardening nonlinearity is increased. Considering these results, for various length-to-radius ratios, the geometrical characteristics also change. Therefore, the natural frequency changes for each length-to-radius ratios. Also, the variation of the length-to-radius ratios causes to change in the illustrated in Fig. 10. As shown in this figure, when $L/$nonlinearity behavior. So the total behavior of the system is a function of these two changes. For instance, in the constant length by increasing the length-to-radius ratios, the nonlinearity decreases until the critical value ($L/R = 13$) and the natural frequency increases, therefore, the hardening behavior decreases, but after this critical value, the nonlinearity doesn't change, while the natural frequency still increases, thus this situation causes to decrease the hardening behavior.

4. Conclusions

An analytical approach was presented to analyze the combination resonances of the FGP cylindrical shells under harmonic excitation. With regard to classical plate theory of shells, von Kármán equation and Hook law, the problem formulation was obtained. According to the Galerkin method, the discretized motion equation is obtained. For obtaining the response of system for combination resonance, the multiple scales method was used. The effects of various porosity distributions, porosity coefficients of cylindrical shell and amplitude excitations were investigated. The principal conclusions can be summarized as follows:

- The hardening nonlinearity behavior of FGP cylindrical shell is more than isotropic cylindrical shell except for type1 (uniform porosity distribution).
- Increasing the porosity coefficients of cylindrical shell leads to increasing nonlinearity behavior.

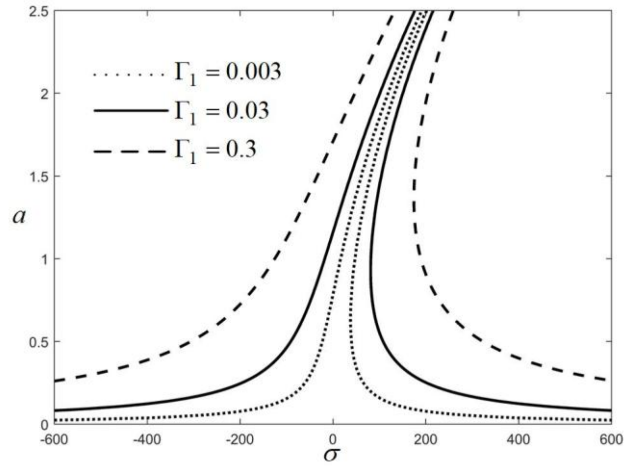

Fig. 7 Effect of excitation amplitude (Γ_1) on the frequency-response of FGP cylindrical shells ($N_0 = 0.4$)

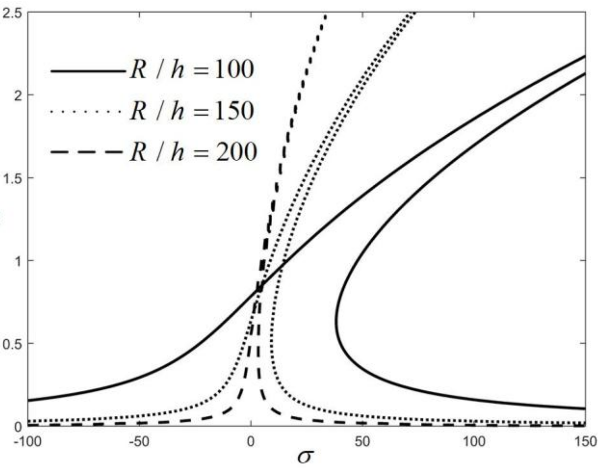

Fig. 9 Effect of radius-to-thickness (R/h) on the frequency-response of FGP cylindrical shells ($N_0 = 0.4$)

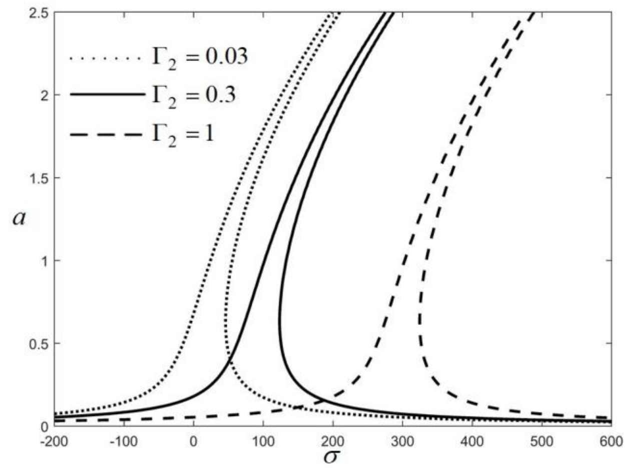

Fig. 8 Effect of excitation amplitude (Γ_2) on the frequency-response of FGP cylindrical shells ($N_0 = 0.4$)

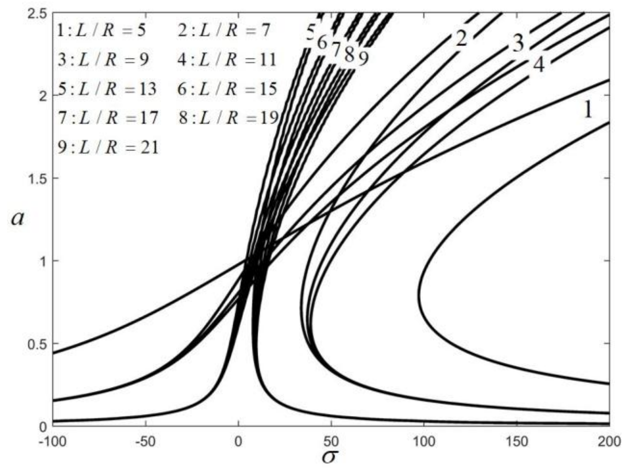

Fig. 10 Effect of length-to-radius (L/R) on the frequency-response of FGP cylindrical shells ($N_0 = 0.4$)

- Increasing of amplitude excitation Γ_1 leads to scaling up the curve of frequency-response.
- By increasing amplitude excitation Γ_2, the jumping phenomenon is transferred to higher values of σ.
- By increasing the radius-to-thickness ratio, the nonlinearity behavior decreases.
- When $L/R=13$, maximum softening nonlinearity is occurred.
- For $L/R > 13$ or $L/R < 13$, the hardening nonlinearity is increased.

References

Abdelhak, Z., Hadji, L., Daouadji, T.H. and Adda, B. (2016), “Thermal buckling response of functionally graded sandwich plates with clamped boundary conditions”, *Smart Struct. Syst., Int. J.*, **18**(2), 267-291. https://doi.org/10.12989/sss.2016.18.2.267

Abe, A., Kobayashi, Y. and Yamada, G. (2007), “Nonlinear dynamic behaviors of clamped laminated shallow shells with one-to-one internal resonance”, *J. Sound Vib.*, **304**, 957-968. https://doi.org/10.1016/j.jsv.2007.03.009

Adim, B. and Daouadji, T.H. (2016), “Effects of thickness stretching in FGM plates using a quasi-3D higher order shear deformation theory”, *Adv. Mater. Res., Int. J.*, **5**(4), 223-244. https://doi.org/10.12989/amr.2016.5.4.223

Adim, B., Daouadji, T.H. and Abbes, B. (2016a), “Buckling analysis of anti-symmetric cross-ply laminated composite plates under different boundary conditions”, *Int. Appl. Mech.*, **52**(6), 661-676. https://doi.org/10.1007/s10778-016-0787-x

Adim, B., Daouadji, T.H., Abbes, B. and Rabahi, A. (2016b), “Buckling and free vibration analysis of laminated composite plates using an efficient and simple higher order shear deformation theory”, *Mech. Indus.*, **17**(5), 512. https://doi.org/10.1051/meca/2015112

Adim, B., Daouadji, T.H. and Rabahi, A. (2016c), “A simple higher order shear deformation theory for mechanical behavior of laminated composite plates”, *Int. J. Adv. Struct. Eng.* (*IJASE*), **8**(2), 103-117. https://doi.org/10.1007/s40091-016-0109-x

Adim, B., Daouadji, T.H., Rabia, B. and Hadji, L. (2016d), “An efficient and simple higher order shear deformation theory for bending analysis of composite plates under various boundary conditions”, *Earthq. Struct., Int. J.*, **11**(1), 63-82. https://doi.org/10.12989/eas.2016.11.1.063

Adim, B., Daouadji, T.H., Rabahi, A. and Abdelouahed, T. (2016e), “An Efficient and Simple Higher Order of Shear Deformation Theory for Static and Free Vibration of Laminated Composite Plates”, *Int. J. Compos. Mater. Matrices*, **2**(1).

Ahmadi, H. (2018), “Nonlinear primary resonance of imperfect spiral stiffened functionally graded cylindrical shells surrounded by damping and nonlinear elastic foundation”, *Eng. Comput.*, 1-15. https://doi.org/10.1007/s00366-018-0679-2

Ahmadi, H. and Foroutan, K. (2019), “Nonlinear primary resonance of spiral stiffened functionally graded cylindrical shells with damping force using the method of multiple scales”, *Thin Wall. Struct.*, **135**, 33-44. https://doi.org/10.1016/j.tws.2018.10.028

Alijani, F., Amabili, M. and Bakhtiari-Nejad, F. (2011), “On the accuracy of the multiple scales method for non-linear vibrations of doubly curved shallow shells”, *Int. J. Nonlin. Mech.*, **46**(1), 170-179. https://doi.org/10.1016/j.ijnonlinmec.2010.08.006

Belica, T. and Magnucki, K. (2006), “Dynamic stability of a porous cylindrical shell”, *Appl. Math. Mech.*, 207-208.

Belica, T., Malinowski, M. and Magnucki, K. (2011), “Dynamic stability of an isotropic metal foam cylindrical shell subjected to external pressure and axial compression”, *J. Appl. Mech.*, **78**(4), 041003. https://doi.org/10.1115/1.4003768

Benferhat, R., Daouadji, T.H. and Mansour, M.S. (2016a), “Free vibration analysis of FG plates resting on an elastic foundation and based on the neutral surface concept using higher-order shear deformation theory”, *Comptes Rendus Mécanique*, **344**(9), 631-641. https://doi.org/10.1016/j.crme.2016.03.002

Benferhat, R., Daouadji, T.H., Mansour, M.S. and Hadji, L. (2016b), “Effect of porosity on the bending and free vibration response of functionally graded plates resting on Winkler-Pasternak foundations”, *Earthq. Struct., Int. J.*, **10**(6), 1429-1449. https://doi.org/10.12989/eas.2016.10.6.1429

Benferhat, R., Hassaine, D., Hadji, L. and Said, M. (2016c), “Static analysis of the fgm plate with porosities”, *Steel Compos. Struct., Int. J.*, **21**(1), 123-136. https://doi.org/10.12989/scs.2016.21.1.123

Bich, D.H., Van Dung, D. and Nam, V.H. (2012), “Nonlinear dynamical analysis of eccentrically stiffened functionally graded cylindrical panels”, *Compos. Struct.*, **94**(8), 2465-2473. https://doi.org/10.1016/j.compstruct.2012.03.012

Bich, D.H., Van Dung, D., Nam, V.H. and Phuong, N.T. (2013), “Nonlinear static and dynamic buckling analysis of imperfect eccentrically stiffened functionally graded circular cylindrical thin shells under axial compression”, *Int. J. Mech. Sci.*, **74**, 190-200. https://doi.org/10.1016/j.ijmecsci.2013.06.002

Breslavsky, I.D. and Amabili, M. (2018), “Nonlinear vibrations of a circular cylindrical shell with multiple internal resonances under multi-harmonic excitation”, *Nonlin. Dyn.*, 1-10.

Brush, D.O. and Almroth, B.O. (1975), *Buckling of Bars, Plates, and Shells*, McGraw-Hill, New York, USA.

Chen, D., Yang, J. and Kitipornchai, S. (2015), “Elastic buckling and static bending of shear deformable functionally graded porous beam”, *Compos. Struct.*, **133**, 54-61. https://doi.org/10.1016/j.compstruct.2015.07.052

Daneshjou, K., Ramezani, H. and Talebitooti, R. (2011), “Wave transmission through laminated composite double-walled cylindrical shell lined with porous materials”, *Appl. Math. Mech.*, **32**, 701-718. https://doi.org/10.1007/s10483-011-1450-9

Daouadji, T.H. and Adim, B. (2016a), “An analytical approach for buckling of functionally graded plates”, *Adv. Mater. Res., Int. J.*, **5**(3), 141-169. https://doi.org/10.12989/amr.2016.5.3.141

Daouadji, T.H. and Adim, B. (2016b), “Theoretical analysis of composite beams under uniformly distributed load”, *Adv. Mater. Res., Int. J.*, **5**(1), 1-9. https://doi.org/10.12989/amr.2016.5.1.001

Daouadji, T.H., Adim, B. and Benferhat, R. (2016a), “Bending analysis of an imperfect FGM plates under hygro-thermo-mechanical loading with analytical validation”, *Adv. Mater. Res., Int. J.*, **5**(1), 35-53. https://doi.org/10.12989/amr.2016.5.1.035

Daouadji, T.H., Benferhat, R. and Adim, B. (2016b), “A novel higher order shear deformation theory based on the neutral surface concept of FGM plate under transverse load”, *Adv. Mater. Res., Int. J.*, **5**(2), 107-120. https://doi.org/10.12989/amr.2016.5.2.107

Djoudi, M.S. and Bahai, H. (2003), “A shallow shell finite element for the linear and non-linear analysis of cylindrical shells”, *Eng. Struct.*, **25**, 769-778. https://doi.org/10.1016/S0141-0296(03)00002-6

Dong, Y.H., Li, Y.H., Chen, D. and Yang, J. (2018), “Vibration characteristics of functionally graded graphene reinforced porous nanocomposite cylindrical shells with spinning motion”, *Compos. Part B-Eng.*, **145**, 1-13. https://doi.org/10.1016/j.compositesb.2018.03.009

Du, C. and Li, Y. (2014), "Nonlinear internal resonance of functionally graded cylindrical shells using the hamiltonian dynamics", *Acta Mech. Solida Sin.*, **27**(6), 635-647. https://doi.org/10.1016/S0894-9166(15)60008-8

Ebrahimi, F. and Habibi, S. (2016), "Deflection and vibration analysis of higher-order shear deformable compositionally graded porous plate", *Steel Compos. Struct., Int. J.*, **20**(1), 205-225. http://dx.doi.org/10.12989/scs.2016.20.1.205

Galeban, M.R., Mojahedin, A., Taghavi, Y. and Jabbari, M. (2016), "Free vibration of functionally graded thin beams made of saturated porous materials", *Steel Compos. Struct., Int. J.*, **21**(5), 999-1016. https://doi.org/10.12989/scs.2016.21.5.999

Gao, K., Gao, W., Wu, B., Wu, D. and Song, C. (2018), "Nonlinear primary resonance of functionally graded porous cylindrical shells using the method of multiple scales", *Thin Wall. Struct.*, **125**, 281-293. https://doi.org/10.1016/j.tws.2017.12.039

Ghadiri, M. and SafarPour, H. (2017), "Free vibration analysis of size-dependent functionally graded porous cylindrical microshells in thermal environment", *J. Therm. Stresses*, **40**(1), 55-71. https://doi.org/10.1080/01495739.2016.1229145

Ghiasian, S.E., Kiani, Y. and Eslami, M.R. (2013), "Dynamic buckling of suddenly heated or compressed fgm beams resting on nonlinear elastic foundation", *Compos. Struct.*, **106**, 225-234. https://doi.org/10.1016/j.compstruct.2013.06.001

Guan, X., Sok, K., Wang, A., Shuai, C., Tang, J. and Wang, Q. (2019), "A general vibration analysis of functionally graded porous structure elements of revolution with general elastic restraints", *Compos. Struct.*, **209**, 277-299. https://doi.org/10.1016/j.compstruct.2018.10.103

Karami, B., Shahsavari, D., Nazemosadat, S.M.R., Li, L. and Ebrahimi, A. (2018), "Thermal buckling of smart porous functionally graded nanobeam rested on kerr foundation", *Steel Compos. Struct., Int. J.*, **29**(3), 349-362. https://doi.org/10.12989/scs.2018.29.3.349

Kitipornchai, S., Chen, D. and Yang, J. (2017), "Free vibration and elastic buckling of functionally graded porous beams reinforced by graphene platelets", *Mater. Design*, **116**, 656-665. https://doi.org/10.1016/j.matdes.2016.12.061

Li, X., Du, C.C. and Li, Y.H. (2018), "Parametric resonance of a fg cylindrical thin shell with periodic rotating angular speeds in thermal environment", *Appl. Math. Model.*, **59**, 393-409. https://doi.org/10.1016/j.apm.2018.01.048

Li, H., Pang, F., Chen, H. and Du, Y. (2019), "Vibration analysis of functionally graded porous cylindrical shell with arbitrary boundary restraints by using a semi analytical method", *Compos. Part B-Eng.*, **164**, 249-264. https://doi.org/10.1016/j.compositesb.2018.11.046

Loy, C.T., Lam, K.Y. and Reddy, J.N. (1999), "Vibration of functionally graded cylindrical shells", *Int. J. Mech. Sci.*, **41**, 309-324. https://doi.org/10.1016/S0020-7403(98)00054-X

Magnucki, K., Malinowski, M. and Kasprzak, J. (2006), "Bending and buckling of a rectangular porous plate", *Steel Compos. Struct., Int. J.*, **6**(4), 319-333. https://doi.org/10.12989/scs.2006.6.4.319

Mirjavadi, S.S., Afshari, B.M., Shafiei, N., Hamouda, A.M.S. and Kazemi, M. (2017), "Thermal vibration of two-dimensional functionally graded (2D-FG) porous Timoshenko nanobeams", *Steel Compos. Struct., Int. J.*, **25**(4), 415-426. https://doi.org/10.12989/scs.2017.25.4.415

Mojahedin, A., Joubaneh, E.F. and Jabbari, M. (2014), "Thermal and mechanical stability of a circular porous plate with piezoelectric actuators", *Acta Mech.*, **225**(12), 3437-3452. https://doi.org/10.1007/s00707-014-1153-x

Pellicano, F. (2007), "Vibrations of circular cylindrical shells: Theory and experiments", *J. Sound Vib.*, **303**(1-2), 154-170. https://doi.org/10.1016/j.jsv.2007.01.022

Pradhan, S.C., Loy, C.T., Lam, K.Y. and Reddy, J.N. (2000), "Vibration characteristics of functionally graded cylindrical shells under various boundary conditions", *Appl. Acoust.*, **61**, 111-129. https://doi.org/10.1016/S0003-682X(99)00063-8

Qin, Z., Chu, F. and Zu, J. (2017), "Free vibrations of cylindrical shells with arbitrary boundary conditions: A comparison study", *Int. J. Mech. Sci.*, **133**, 91-99. https://doi.org/10.1016/j.ijmecsci.2017.08.012

Rodrigues, L., Gonçalves, P.B. and Silva, F.M.A. (2017), "Internal resonances in a transversally excited imperfect circular cylindrical shell", *Pro. Eng.*, **199**, 838-843. https://doi.org/10.1016/j.proeng.2017.09.010

Rossikhin, Y.A. and Shitikova, M.V. (2015), "Nonlinear dynamic response of a fractionally damped cylindrical shell with a three-to-one internal resonance", *Appl. Math. Comput.*, **257**, 498-525. https://doi.org/10.1016/j.amc.2015.01.018

Sewall, J.L. and Naumann, E.C. (1968), "An experimental and analytical vibration study of thin cylindrical shells with and without longitudinal stiffeners", *NASA Technical Note D-4705*.

Shen, H.-S. and Xiang, Y. (2012), "Nonlinear vibration of nanotube-reinforced composite cylindrical shells in thermal environments", *Comput. Methods Appl. Mech. Eng.*, **213**, 196-205. https://doi.org/10.1016/j.cma.2011.11.025

Sheng, G.G. and Wang, X. (2018a), "The dynamic stability and nonlinear vibration analysis of stiffened functionally graded cylindrical shells", *Appl. Math. Model.*, **56**, 389-403. https://doi.org/10.1016/j.apm.2017.12.021

Sheng, G.G. and Wang, X. (2018b), "Nonlinear vibrations of fg cylindrical shells subjected to parametric and external excitations", *Compos. Struct.*, **191**, 78-88. https://doi.org/10.1016/j.compstruct.2018.02.018

Tesar, A. (1985), "Nonlinear three-dimensional resonance analysis of shells", *Comput. Struct.*, **21**, 797-805. https://doi.org/10.1016/0045-7949(85)90156-7

Volmir, A.S. (1972), *Non-linear dynamics of plates and shells*, Science Edition M, USSR.

Wang, Y. and Wu, D. (2017), "Free vibration of functionally graded porous cylindrical shell using a sinusoidal shear deformation theory", *Aerosp. Sci. Tech.*, **66**, 83-91. https://doi.org/10.1016/j.ast.2017.03.003

Yang, J., Chen, D. and Kitipornchai, S. (2018), "Buckling and free vibration analyses of functionally graded graphene reinforced porous nanocomposite plates based on Chebyshev-Ritz method", *Compos. Struct.*, **193**, 281-294. https://doi.org/10.1016/j.compstruct.2018.03.090

Zare Jouneghani, F., Dimitri, R., Bacciocchi, M. and Tornabene, F. (2017), "Free vibration analysis of functionally graded porous doubly-curved shells based on the first-order shear deformation theory", *Appl. Sci.*, **7**(12), 1252. https://doi.org/10.3390/app7121252

Zhang, L., Song, Z. and Liew, K. (2017), "Modeling aerothermoelastic properties and active flutter control of nanocomposite cylindrical shells in supersonic airflow under thermal environments", *Comput. Methods Appl. Mech. Eng.*, **325**, 416-433. https://doi.org/10.1016/j.cma.2017.07.014

Zhang, W., Liu, T., Xi, A. and Wang, Y.N. (2018), "Resonant responses and chaotic dynamics of composite laminated circular cylindrical shell with membranes", *J. Sound Vib.*, **423**, 65-99. https://doi.org/10.1016/j.jsv.2018.02.049

Zhao, J., Wang, Q., Deng, X., Choe, K., Xie, F. and Shuai, C. (2019a), "A modified series solution for free vibration analyses of moderately thick functionally graded porous (FGP) deep curved and straight beams", *Compos. Part B-Eng.*, **165**, 155-166. https://doi.org/10.1016/j.compositesb.2018.11.080

Zhao, J., Wang, Q., Deng, X., Choe, K., Zhong, R. and Shuai, C. (2019b), "Free vibrations of functionally graded porous rectangular plate with uniform elastic boundary conditions", *Compos. Part B-Eng.*, **168**, 106-120.

https://doi.org/10.1016/j.compositesb.2018.12.044

Zhao, J., Xie, F., Wang, A., Shuai, C., Tang, J. and Wang, Q. (2019c), "A unified solution for the vibration analysis of functionally graded porous (FGP) shallow shells with general boundary conditions", *Compos. Part B-Eng.*, **156**, 406-424. https://doi.org/10.1016/j.compositesb.2018.08.115

Zhao, J., Xie, F., Wang, A., Shuai, C., Tang, J. and Wang, Q. (2019d), "Dynamics analysis of functionally graded porous (FGP) circular, annular and sector plates with general elastic restraints", *Compos. Part B-Eng.*, **159**, 20-43. https://doi.org/10.1016/j.compositesb.2018.08.114

Zhao, J., Xie, F., Wang, A., Shuai, C., Tang, J. and Wang, Q. (2019e), "Vibration behavior of the functionally graded porous (FGP) doubly-curved panels and shells of revolution by using a semi-analytical method", *Compos. Part B-Eng.*, **157**, 219-238. https://doi.org/10.1016/j.compositesb.2018.08.087

CC

Appendix

$$
\begin{aligned}
A &= J_{11}^{*} m^4 \pi^4 + \left(J_{33}^{*} - J_{12}^{*} - J_{21}^{*}\right) m^2 n^2 \pi^2 \lambda^2 + J_{22}^{*} n^4 \lambda^4 \\
B &= J_{21}^{**} m^4 \pi^4 + \left(J_{11}^{*} + J_{22}^{*} - 2J_{36}^{**}\right) m^2 n^2 \pi^2 \lambda^2 \\
&\quad + J_{12}^{**} n^4 \lambda^4 - \frac{L^2}{R} m^2 n^2 \\
B^{*} &= A_{21}^{*} m^4 \pi^4 + \left(A_{11}^{*} + A_{22}^{*} - 2J_{36}^{**}\right) m^2 n^2 \pi^2 \lambda^2 \\
&\quad + J_{12}^{**} n^4 \lambda^4 - \frac{L^2}{R} m^2 n^2 \\
D &= A_{11}^{**} m^4 \pi^4 + \left(A_{12}^{**} + A_{21}^{**} + 4A_{36}^{**}\right) m^2 n^2 \pi^2 \lambda^2 \\
&\quad + A_{22}^{**} n^4 \lambda^4 \\
G &= \left(\frac{n^4 \lambda^4}{16 J_{11}^{*}} + \frac{m^4 \pi^4}{16 J_{22}^{*}}\right) \\
\lambda &= \frac{L}{R}
\end{aligned}
\tag{A1}
$$

where

$$
\begin{gathered}
\Delta = J_{11} J_{22} - J_{12} J_{21},\ \ J_{22}^{*} = \frac{J_{22}}{\Delta},\ \ J_{12}^{*} = \frac{J_{12}}{\Delta} \\
J_{11}^{*} = \frac{J_{11}}{\Delta},\ \ I_{21}^{*} = \frac{J_{21}}{\Delta},\ \ J_{33}^{*} = \frac{1}{J},\ \ J_{36}^{*} = \frac{J_{36}}{J_{33}} \\
J_{11}^{**} = J_{22}^{*} J_{14} - J_{12}^{*} J_{24},\ \ J_{12}^{**} = J_{22}^{*} J_{15} - J_{12}^{*} J_{25} \\
J_{21}^{**} = J_{11}^{*} J_{24} - J_{21}^{*} J_{14},\ \ J_{22}^{**} = J_{11}^{*} J_{25} - J_{21}^{*} J_{15} \\
A_{11}^{*} = J_{22}^{*} J_{14} - J_{21}^{*} J_{15},\ \ A_{21}^{*} = J_{11}^{*} J_{15} - J_{12}^{*} J_{14} \\
A_{12}^{*} = J_{22}^{*} J_{24} - J_{21}^{*} J_{25},\ \ A_{22}^{*} = J_{11}^{*} J_{25} - J_{12}^{*} J_{24} \\
A_{11}^{**} = J_{11}^{**} J_{14} - J_{21}^{**} J_{15} - J_{41} \\
A_{12}^{**} = J_{12}^{**} J_{14} - J_{22}^{**} J_{15} - J_{42} \\
A_{21}^{**} = J_{11}^{**} J_{24} - J_{21}^{**} J_{25} - J_{51} \\
A_{22}^{**} = J_{12}^{**} J_{24} - J_{22}^{**} J_{25} - J_{52} \\
A_{36}^{**} = J_{36}^{**} J_{36} - J_{63}
\end{gathered}
\tag{A2}
$$

where

$$
\begin{gathered}
J_{11} = \frac{E_1}{1-\nu^2},\ \ J_{12} = \frac{E_1 \nu}{1-\nu^2},\ \ J_{14} = \frac{E_2}{1-\nu^2} \\
I_{15} = \frac{E_2 \nu}{1-\nu^2},\ \ I_{21} = \frac{E_1 \nu}{1-\nu^2},\ \ I_{22} = \frac{E_1}{1-\nu^2} \\
I_{24} = \frac{E_2 \nu}{1-\nu^2},\ \ I_{25} = \frac{E_2}{1-\nu^2},\ \ I_{33} = \frac{E_1}{2(1+\nu)} \\
I_{36} = \frac{E_2}{2(1+\nu)},\ \ I_{41} = \frac{E_3}{1-\nu^2},\ \ I_{42} = \frac{E_3 \nu}{1-\nu^2} \\
I_{51} = \frac{E_3 \nu}{1-\nu^2},\ \ I_{55} = \frac{E_3}{1-\nu^2},\ \ I_{63} = \frac{E_3}{2(1+\nu)}
\end{gathered}
\tag{A3}
$$

where

$$
\left(E_1, E_2, E_3\right) = \int_{-h/2}^{h/2} E(z)\left(1, z, z^2\right) dz \tag{A4}
$$